

CONTRIBUTION INDEX OF LAND COVER AND LAND SURFACE TEMPERATURE CHANGES IN UPPER HILL NAIROBI, KENYA

P.W. Mwangi^{1,*}, F.N. Karanja², P.K. Kamau¹, S.C. Letema³

¹ Dept. of Urban & Regional Planning, Kenyatta University, Nairobi, Kenya- (mwangi.patricia, kamau.peter)@ku.ac.ke

² Dept. of Geospatial Engineering, University of Nairobi, Kenya- faithkaranja@uonbi.ac.ke

³ Dept. of Environmental Planning & Management, Kenyatta University, Nairobi, Kenya- letema.sammy@ku.ac.ke

Commission III, WG III/7

KEY WORDS: Urban Heat Island, Land Surface Temperature, Land Cover, Contribution Index, Albedo

ABSTRACT:

Urban heat island is the difference in thermal temperature between rural and urban areas. The urbanization process alters the material type with impervious surfaces being absorbers of incoming radiation during the day and emitting it at night. The research involved the use of time-series satellite imagery from Sentinel, Landsat, ASTER and MODIS for the period 1986, 1995, 2000, 2005, 2011, 2015 and 2017 over the Upper Hill, Nairobi. Morning, afternoon and night land surface temperatures (LST) were calculated for each of these years and analyzed together with the land cover. The mean albedo was calculated to determine the relationship between each land cover and mean LST. The contribution index was calculated to determine whether a land contributed positively or negatively to the mean LST in Upper Hill. Results indicated that built-up land cover had increased from 1986 to 2017 by 0.86% per annum while forest land cover had decreased by 0.99% per annum. Sparse grassland had higher albedo and LST values of 0.81 and 27.9 °C respectively, whereas water had lower albedo and LST values of 0.09 and 25.1 °C. Water had the lowest mean LST during the day but highest mean LST in the afternoon and night in each of the years due to its high thermal capacity. Bare ground tends to have a higher contribution index compared to other land covers, while forest land cover has a negative contribution index, indicating the impact land cover types have on LST and the urban heat island effect.

1. INTRODUCTION

Human activities have led to irreversible changes to the ecosystem and it is likely that further damage will occur (Schipper *et al.*, 2010). Perceived changes in temperature, sea-level rise have been reported in many cities and this has been attributed to climate change (Carmin *et al.*, 2012). Whether or not causes of climate change can be attributed to anthropogenic activities, it is evident that there are new climate and weather patterns. This potentially puts urban residents at risk, affecting their health and wellbeing, while stressing the environment, buildings and other assets (Carmin *et al.*, 2012).

The earth's energy budget is affected by human activities that alter properties of the land surface and pollutant emissions (Wu & Lung, 2016). In cities, urban heat islands (UHI) has been intensively studied and involves computing the differences in surface and air temperature between nearby rural and urban areas (Zhan *et al.*, 2015). Boundary layer urban heat island (BUHI), canopy urban heat island (CUHI) and surface urban heat island (SUHI) are the main UHI identified, with SUHI being great both day and night (James, 2000). Differences in cooling between urban and rural areas results to formation of urban heat (UH) in the air (Voogt, 2007). The land surface temperature (LST), which considered an important parameter in urban climate, directly controls UHI (Feizizadeh & Blaschke, 2013).

Spatial metrics enable correct interpretation about patterns and structure of changes such as in patch sizes, landscape fragmentation

etc. (Koukoulas *et al.*, 2008). Spatial metrics are impactful tools when combined with remote sensing techniques to link urban land-use patterns and dynamic processes (Zhao & Murayama, 2011). Studying patterns of land cover changes enables one to quantify the effects and patterns of these changes. The urbanization process alters the surface albedo, leading to increased air temperatures compared to rural areas, resulting to UHI effect (Bhargava & Bhargava, 2018). Vegetation is thus considered an important part of the urban landscape due to its effects on air quality, temperature and air humidity (Mishra, 2009). Tree cover and natural vegetation, through the evapotranspiration process, effectively cools surrounding areas (Grover & Singh, 2015).

The effects of increased urbanization, on land surface temperature needs to be evaluated. Contribution of these changes on the UHI is important in developing adaptive and mitigative measures on the climate change challenges facing the world in the 21st century and in future.

2. METHODOLOGY

2.1 Study Area

The study area is Upper Hill, Nairobi Kenya and is 4.2 square kilometers and has an average altitude of 1700 meters above sea level. Nairobi has two rainy seasons: 'long' rainy season in March-May (MAM) and a 'short' rainy season in October-December (OND). Predominant winds are easterlies which are linked to

* Corresponding author

moisture inflow from the Indian ocean into the country (Ongoma *et al.*, 2016). Average temperature and rainfall data between 1984-2013 from Wilson meteorological station indicates that the coldest season occurs in June-August (JJA) (Figure 1) due to the advection of cold air from the southern hemisphere (Ongoma *et al.*, 2016). Higher temperatures occur in February-March (Figure 1).

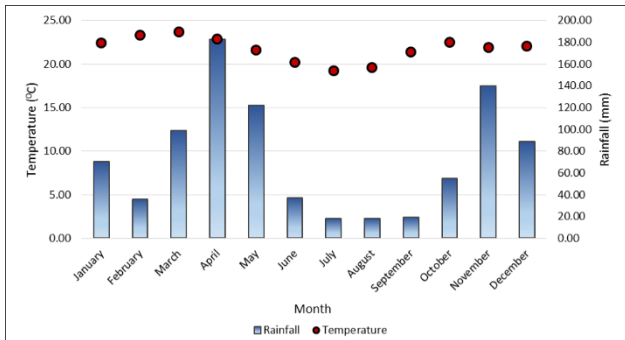


Figure 1: Mean monthly temperature and rainfall from Wilson Station, Nairobi

Upper Hill has seen rapid transformation from residential use to commercial, office and government institutions, with high-rise buildings being the main development (Mwangi *et al.*, 2020).

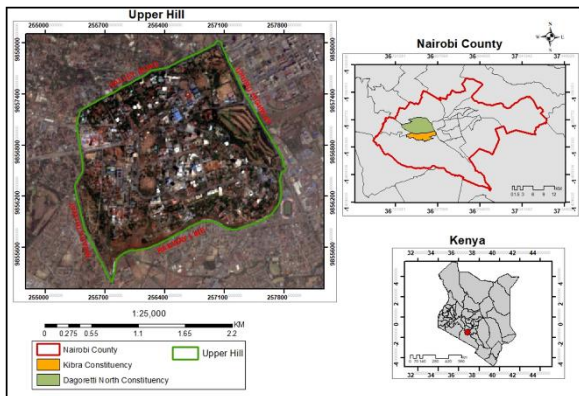


Figure 2: Location of Upper Hill in Nairobi (Sentinel-2 (ESA) imagery courtesy of USGS, 2017)

Changes in zoning policies on plot ratio (PR) and ground coverage ratio (GCR) have contributed to land use changes and eventual land cover changes. Proximity to the central business district (CBD) has also contributed to its transformation with pressures from businesses relocating and eventual construction of high-rise buildings (Mwangi *et al.*, 2020; Kiai *et al.*, 2008). The transformation has resulted in urban greenery being transformed to impervious surfaces (Karanja & Matara, 2013), resulting to increased surface temperatures. Effects of land cover changes on the albedo and eventual surface temperature needs to be modelled for necessary mitigative measures. Lack of indicators on the interaction of land cover with incoming radiation becomes a challenge in formulating policies on dealing with changing climate in urban areas.

2.2 Processing of Satellite Imagery

Satellite imagery was downloaded from USGS website and processed in respect to the datasets required for the analysis. A summary of the image processing processes is shown in figure 3.

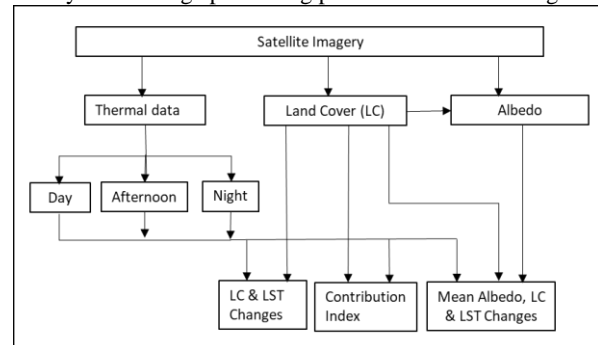


Figure 3: Flowchart of satellite image processing

Satellites acquired for the analysis included: Landsat 5, 7 and 8; ASTER; MODIS and Sentinel-2 imagery. Sentinel-2 was only used in land cover analysis as it does not have thermal bands. All downloaded imagery was transformed from UTM WGS84 Zone 37 N/S projection system to UTM Arc1960 South in ArcGIS 10.7, after which the area of interest (AOI) (Figure 2) was clipped.

2.3 Land Cover Classification

Cloud-free level-1 tier satellite imagery was acquired from USGS for different sensors on different days in the months of January and February. These are considered warm months in the year in Kenya (Table 1). These datasets were also used in determining the LST and albedo over Upper Hill.

Date	Satellite	Time of Day	Resolution
05-01-1986	Landsat 5 TM	10:00am	30m
30-01-1995	Landsat 5 TM	10:00am	30m
21-02-2000	Landsat 7 ETM+	10:00am	30m
18-02-2005	ASTER	10:30am	15m
25-01-2011	ASTER	10:30am	15m
11-02-2017	Landsat 8 OLR/ TIR	10:00am	30m
08-02-2017	Sentinel-2	10:30am	10m

Table 1: Satellite imagery acquired

Cloud-free satellite imagery collected during the cold seasons was not available within the same years as datasets collected in table 1. Hence only imagery collected in January and February were used. Five land cover were identified following the Food and Agriculture Organization (FAO) land cover classification system (LCCS) in Upper Hill namely: forest, built-up, water, open grassland and sparse grassland. These were used to define training sites. Cropped imagery and training sites were imported in R studio for land cover classification using random forests. Classification accuracy was determined using the confusion matrix. Land cover changes were carried out between the years 1986-1995, 1995-2000, 2000-2005, 2005-2011 and 2011-2017. Land cover changes included: vegetated to built-up, forest to open grassland, forest to sparse grassland and no change. A minimum mapping unit (MMU) was applied to eliminate small land cover (LC) pixels, where 1986 and

1995, 1995 and 2000 an MMU of 0.09 Ha was used as the spatial resolution of Landsat is 30m. In 2000-2005 and 2005-2011 an MMU of 0.045 Ha was applied as ASTER has a spatial resolution of 15m. In 2011-2017 an MMU of 0.0225 Ha was applied as Sentinel's spatial resolution is 10m. LST changes between the same year intervals were spatially linked to the land cover changes. This was to determine whether changes in land cover had subsequent effects on the changes in LST in areas where changes had been mapped.

2.4 Land Surface Temperature Computation

Day, afternoon and night LST was analyzed to determine changes in minimum, maximum and mean temperatures. Satellite imagery indicated in table 1 were used to determine the morning LST, except for Sentinel-2.

Date	Satellite	Time of Day	Resolution
18-02-2005	MODIS (Aqua)	13:30pm	1Km
25-01-2011	MODIS (Aqua)	13:30pm	1Km
10-02-2017	MODIS (Aqua)	13:30 pm	1Km
26-02-2000	MODIS (Terra)	22:30 pm	1Km
18-02-2005	MODIS (Terra)	22:30 pm	1Km
25-01-2011	MODIS (Terra)	22:30 pm	1Km
10-02-2017	MODIS (Terra)	22:30 pm	1Km

Table 2: Satellite imagery acquired for LST analysis

Available satellite imagery for afternoon and night time was for the years 2000, 2005, 2011 and 2017. LST from Landsat 5, Landsat 7 and Landsat 8 were derived using the 'single channel method' in ArcMap 10.7 where one band was used (Cristóbal *et al.*, 2018). ASTER imagery was processed in ENVI 5.1 where all thermal bands were analyzed together using the three-step method to calculate the LST. Landsat 5 TM was converted to Landsat 7 ETM+ equivalent data to compute the top of atmosphere (TOA) (Equation 1). This has been elaborated by Vogelmann *et al.*, (2001), with Firl & Carter (2011) describing how one can compute to Landsat 5 TM from Landsat 7 ETM+.

$$DN7 = (Slope_y * DN5) + Intercept_y \quad (1)$$

Where $DN7$ and $DN5$ are the digital numbers of Landsat 7 ETM+ and Landsat 5 TM respectively.

The slope and intercept values are band specific and these have been calculated by Firl & Carter (2011). Band 6, the thermal band, was not recalculated.

2.4.1 Converting to Top of Atmosphere (TOA) from DN:

The digital number (DN) spectral information was transformed into TOA radiometric values for Landsat 7 (Equation 2) and Landsat 8 (Equation 3). Band 6a in Landsat 7 was used for the analysis as it has a low radiance variance compared to band 6b (Patricia Wanjiku Mwangi, Karanja, & Kamau, 2018).

$$L_{y'} = \left(\frac{L_{max} - L_{min}}{Q_{calmax} - Q_{calmin}} \right) * (Q_{cal} - Q_{calmin}) + L_{min} \quad (2)$$

Where:

- $L_{y'}$ is the spectral radiance
- Q_{calmin} is minimum quantized calibrated pixel value in DN
- Q_{calmax} is maximum quantized calibrated pixel value in DN

- Q_{cal} is pixel DN value
- L_{min} is minimum radiance detected by sensor
- L_{max} is maximum radiance detected by sensor

Band 10 in Landsat 8 is recommended for calculating TOA radiance values as band 11 has been contaminated with stray light, thus making it unsuitable (USGS, 2016).

$$L_{y''} = M_L Q_{cal} + A_L \quad (3)$$

Where:

- $L_{y''}$ is TOA radiance ($W / (m^2 * sr * \mu m)$)
- M_L is Multiplicative rescaling factor (RADIANCE_MULT_BAND_x where x is the band number) and is band specific
- Q_{cal} is digital number (DN)
- A_L is Additive rescaling factor (RADIANCE_ADD_BAND_x where x is the band number) which is band specific

Conversion to true TOA, using the solar elevation angle from metadata, was carried out for all bands except thermal bands (USGS, 2016).

$$R_{TOAy} = \frac{\pi L_{y''} d^2}{E_{sun_y} \sin \theta_{SE}} \quad (4)$$

Where:

- R_{TOAy} TOA planetary reflectance for band y and is unitless
- π 3.141592654
- d Earth_Sun_distance in astronomical units
- E_{sun_y} Band specific mean solar exoatmospheric irradiance
- θ_{SE} Sun elevation angle from metadata; in degrees and converted to radians

For Landsat 8, TOA was calculated using scaling factors (USGS, 2016) from metadata (Equation 5):

$$\rho_{y'} = M'_L Q_{cal} + A'_L \quad (5)$$

Where:

- $\rho_{y'}$ TOA reflectance and is unitless
- M'_L Multiplicative rescaling factor (REFLECTANCE_MULT_BAND_x where x is band number) and is band specific
- Q_{cal} Digital number (DN)
- A'_L Additive rescaling factor (REFLECTANCE_ADD_BAND_x where x is the band number) and is band specific

Sun angle correction for TOA reflectance results in true TOA reflectance (Equation 6):

$$\rho_{\lambda} = \frac{\rho_{y'}}{\sin \theta} \quad (6)$$

Where:

- ρ_y TOA planetary reflectance in Landsat 8 and is unitless
- θ Solar elevation angle from metadata and is converted to radians

The effective temperature viewed by a satellite with an assumption of unity emission is the at-satellite brightness. This is calculated for

thermal bands only in equation for both Landsat 7 and Landsat 8 (Equation 7).

$$T_{SB} = K_2 / \ln\left(\frac{K_1}{L_y} + 1\right) \quad (7)$$

Where:

- T_{SB} At-satellite-brightness temperature in degrees Celsius
- K_1 Thermal conversion constant (K1_CONSTANT_BAND_m, where m is 6a in Landsat 7 and 10 in Landsat 8) and is band specific
- K_2 Thermal conversion constant (K2_CONSTANT_BAND_m, where m is 6a in Landsat 7 and 10 in Landsat 8) and is band specific
- L_y TOA radiance for Landsat 7 or Landsat 8

2.4.2 Emissivity: Red (R) and near-infrared (NIR) reflectance values (Equation 4) were used to calculate normalized difference vegetated index (NDVI) for Landsat 7 and Landsat 8 (Equation 8):

$$NDVI = \frac{NIR-R}{NIR+R} \quad (8)$$

Vegetation portion was calculated as (Equation 9):

$$V_p = \left(\frac{NDVI-NDVI_{min}}{NDVI_{max}-NDVI_{min}}\right)^2 \quad (9)$$

Where:

- V_p Vegetation portion
- NDVI Normalized difference vegetation index
- $NDVI_{min}$ Minimum NDVI for pure soil, normally at 0.2
- $NDVI_{max}$ Maximum NDVI for pure vegetation, normally at 0.5

Land surface emissivity (LSE) was computed as (Equation 10):

$$LSE = 0.004 * V_p + 0.986 \quad (10)$$

2.4.3 Land Surface Temperature: The land surface emissivity and at-satellite brightness were used to calculate the land surface temperature in Celsius (Equation 11):

$$LST = \left[\frac{T_{SB}}{(1+(\lambda * \frac{T_{SB}}{\rho}) * \ln(LSE))} \right] - 273.15 \quad (11)$$

Where:

- LST Land surface temperature
- T_{SB} At-satellite brightness temperature
- λ Wavelength of emitted radiance ($\lambda = 11.5\mu\text{m}$)
- ρ $h * \frac{c}{\sigma}$ ($1.438 * 10^{-2} \text{ m K}$)
- σ Boltzmann's constant ($1.38 * 10^{-23} \text{ J K}^{-1}$)
- h Planck's constant ($6.26 * 10^{-34} \text{ J s}$)
- c Velocity of light ($2.998 * 10^8 \text{ m s}^{-1}$)

2.5 Albedo Computation

The albedo, which is the surface material type of a surface, for each of the five land cover classes for the years 1986, 1995, 2000, 2005, 2011 and 2017 was calculated using the satellite imagery Landsat 7 (Equation 12), Landsat 8 (Equation 13), and ASTER (Equation 14 & 15). The relationship between the five land cover, mean morning LST and albedo for each year was determined.

$$A_{L7} = \frac{0.356\alpha_1+0.13\alpha_3+0.373\alpha_4+0.085\alpha_5+0.072\alpha_7-0.0018}{0.356+0.130+0.373+0.085+0.072} \quad (12)$$

$$A_{L8} = \frac{0.116\alpha_2+0.321\alpha_3+0.355\alpha_4-0.027\alpha_5+0.150\alpha_7-0.0037}{0.116+0.321+0.355-0.027+0.150} \quad (13)$$

$$A_{ASTER05} = 0.484\alpha_{A1} + 0.335\alpha_{A3} - 0.324\alpha_{A5} + 0.551\alpha_{A6} + 0.305\alpha_{A8} - 0.367\alpha_{A9} \quad (14)$$

$$A_{ASTER11} = 0.697\alpha_{A1} + 0.298\alpha_{A3} + 0.008 \quad (15)$$

Where:

- A_{L7} and A_{L8} are values of surface albedo for Landsat 7 and 8
- $A_{ASTER05}$ are surface albedo values for ASTER 2005 imagery
- $A_{ASTER11}$ are surface albedo values for ASTER 2011 imagery
- α_i are Landsat TOA reflectance values for bands i
- α_{Ax} are ASTER reflectance values for band x

2.6 Contribution Index Computation

The contribution index (CI) indicates whether a land cover type contributes positively or negatively to the surface temperature in the study area. A positive value indicates that the land cover positively contributes to the LST in the study area while negative values indicate that it negatively contributes to the surface temperature and therefore lowers it. CI was determined using equation 16.

$$CI = A * T_D \quad (16)$$

Where A is a ratio between the land cover area and the total area of the study area, while T_D is the difference in mean temperature between a land cover and the study area.

3. RESULTS

3.1 Land Cover Change

Land cover changes from 1986 to 2017 showed an increase in built-up land cover of 0.86% per annum while forest land cover decreased by 0.99% per annum. Water bodies did not show any significant changes as there is only one within the study area used for recreational purposes. Open and sparse grassland showed alternating fluctuations between the years due to changes in climatic conditions (Table 3).

Land Cover	1986	1995	2000	2005	2011	2017
Built-up	23.2	25.1	32.5	37.8	42.8	50.0
Forest	46.9	41.2	29.6	23.2	24.8	16.1
Sparse grassland	17.7	11.1	14.2	27.8	22.6	21.2
Water	0.2	0.2	0.5	0.2	0.4	0.2
Open grassland	12.0	22.4	23.3	10.9	9.4	12.4

Table 3: Percentage change in land cover from 1986 to 2017

3.2 LST and Land Cover

Analysis of LST acquired in the morning indicated that the years 2000, 2005 and 2011 had higher temperature, with 2005 being the highest compared to other years analyzed (Figure 4).

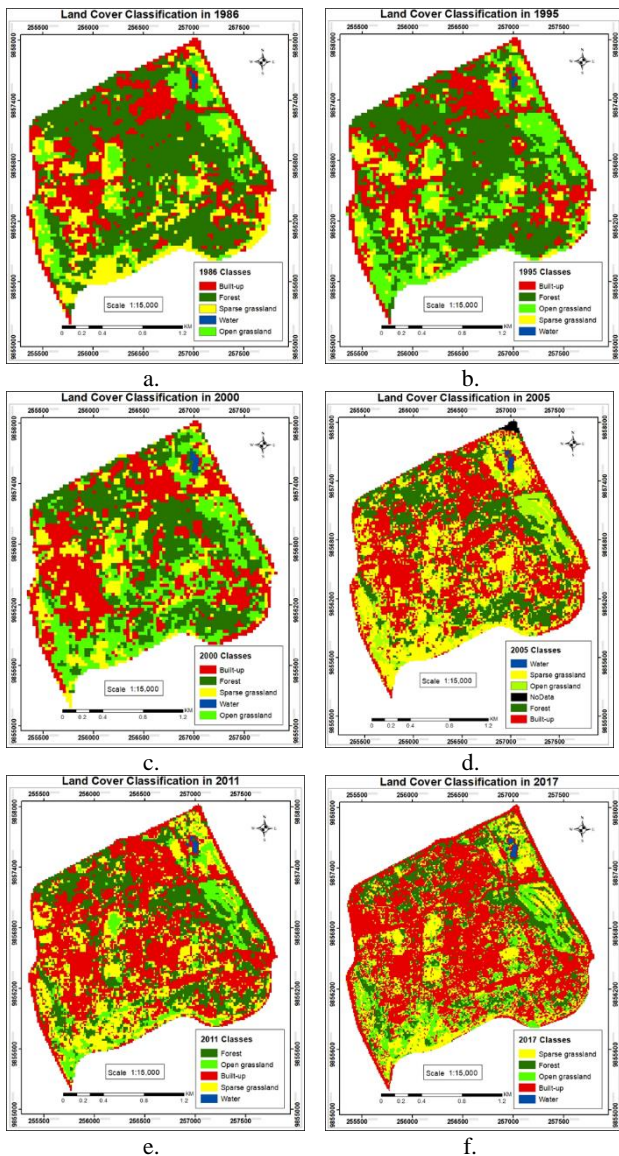


Figure 4: Land cover classification for 1986(a), 1995(b), 2000(c), 2005(d), 2011(e) and 2017(f), in Upper Hill, Nairobi

This was attributed to dry conditions in each of these years, with 2010 to 2011 drought being the worst drought in 60 years (Mbogo *et al.*, 2015). 1986 had lower mean LST which indicated increased mean LST thus changing climatic conditions (Table 4).

Year	1986	1995	2000	2005	2011	2017
Min (°C)	19.98	21.49	24.97	28.17	24.26	23.96
Max (°C)	27.67	29.37	38.83	41.44	34.39	32.33
Mean (°C)	24.35	25.28	32.52	35.00	39.14	28.10

Table 4: Minimum, maximum and mean LST from 1986 to 2017

In all years analyzed (Figure 6), sparse grassland had higher LST compared to other land cover with 25.5°C in 1986 (figure 6a) and 35.7 °C in 2005 (figure 6d).

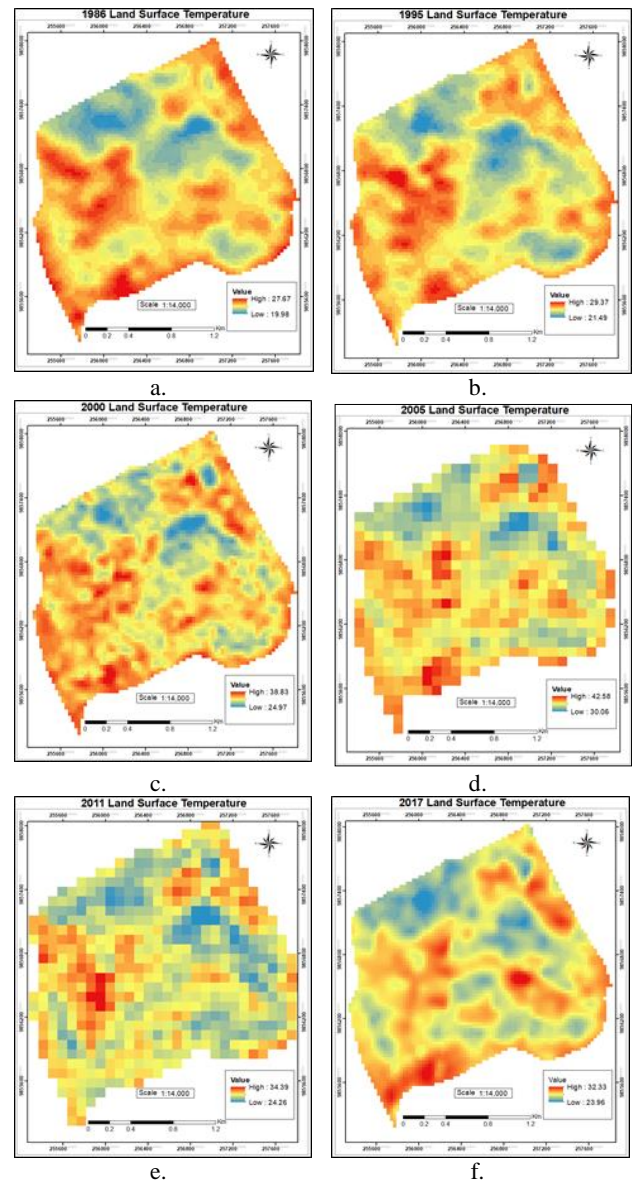


Figure 5: Morning land surface temperature for 1986(a), 1995(b), 2000(c), 2005(d), 2011(e) and 2017(f), in Upper Hill, Nairobi

Open grassland land had the same LST with built-up areas, except for in 2005 where built-up areas had a mean LST of 35.4°C compared to 34.5°C in open grassland. Bare ground and that which does not have much vegetative cover tends to warm up faster compared to other land cover as it reflects incoming radiation. However, the amount of moisture in the soil affects the surface temperature (Tian *et al.*, 2012). Forest land cover and water bodies had a low LST with a mean of 23.5 °C in 1986. Forests have a cooling effect due to evapotranspiration while water takes longer to warm up due to its large thermal heat capacity thus taking longer to warm up. Water had the lowest temperature ranges indicating minimal differences between the maximum and minimum calculated LST, while forests had the largest ranges in all years (figure 6).

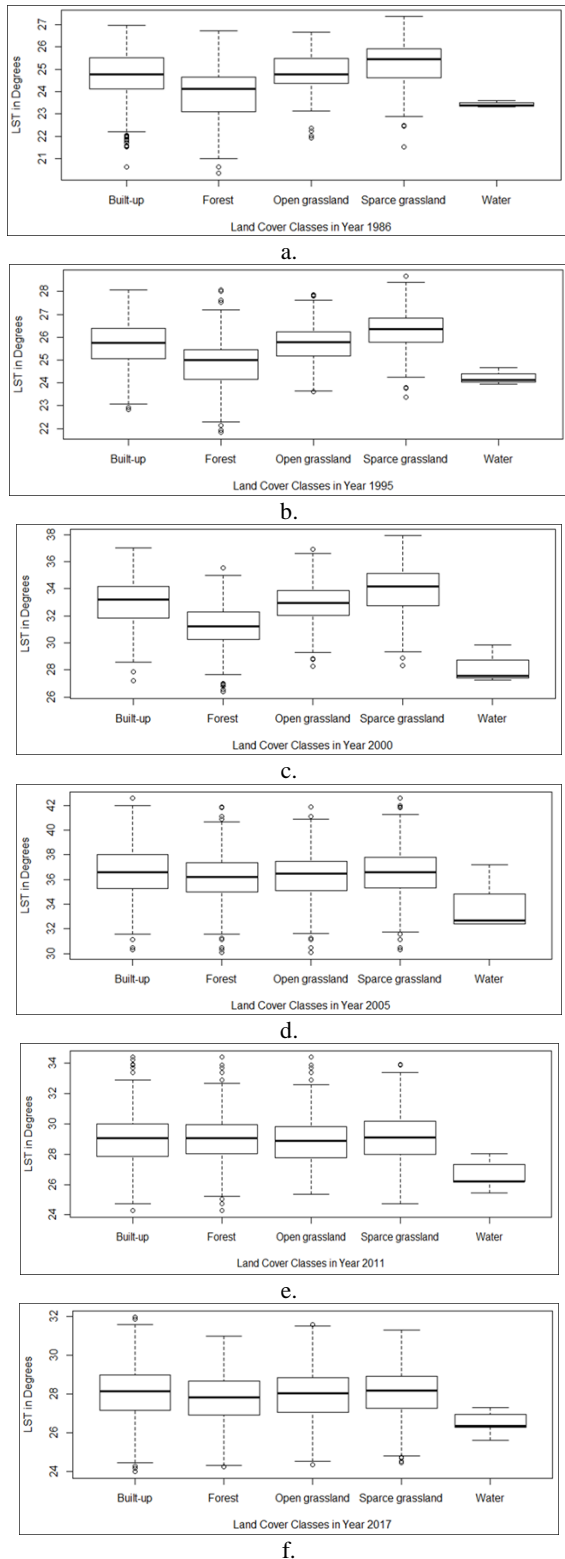


Figure 6: Mean LST of land cover from 1986 to 2017

Mean afternoon and night LST extracted from MODIS imagery indicated a decrease in LST from the year 2000 to 2017 (Table 5). This was attributed to the dry conditions experienced in 2000, 2005

and 2011 which indicates a similar trend with the morning LST (Table 4).

Year	Afternoon Mean (°C)	Night Mean (°C)
2000	-	18.87
2005	45.49	18.80
2011	38.90	16.45
2017	40.41	13.77

Table 5: Mean afternoon and night LST from 2000 to 2017

Mean afternoon and night time temperatures were compared with each land cover for the years 2005, 2011, 2015 and 2017 (Figure 7). Results showed that water had the highest LST in all years, both afternoon and night. Its high thermal capacity allows it to absorb and store heat from incoming solar radiation, slowly emitting it in form of long wave radiation. This creates a warming effect in the surrounding environments. This is contrary to LST of water taken in the morning at 10:00 am where it had the lowest mean LST (Figure 6).

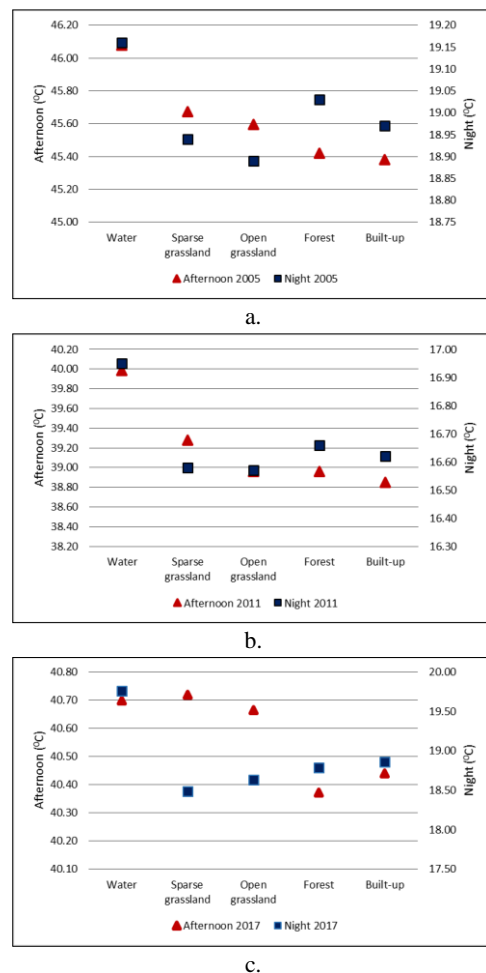


Figure 7: Mean afternoon and night LST of land cover

In the afternoon, forests LST was slightly higher than built-up, which had the lowest LST in 2005 and 2011, while in 2017, forest LC had the lowest LST at 40.37°C. At night, forest land cover had higher LST than built-up, open and closed grassland. Forests also

have a warming effect as seen in the figure 7, as they release heat energy that has been stored during the day (Li *et al.*, 2015). However, this warming effect tends to be lower than its cooling effect during the day. Trapped humidity and heat within urban canopy layers results in cool day-time and warmer night-time temperatures of forests (Sodoudi *et al.*, 2018). In the afternoon, sparse and open grassland had lower LST than water since heat is conducted downwards during the day in soils and conducted upwards at night. This means that at night, open grounds tend to cool faster than other land covers (Sodoudi *et al.*, 2018). This can be noted in night LST where open and sparse grassland have the lowest LST in all years (Figure 7).

Land Cover	1986-1995		1995-2000		2000-2005		2005-2011		2011-2017	
	Area (%)	Temp (°C)								
Vegetated to built-up	7.45	3.78	11.63	22.19	14.08	12.03	12.08	-22.00	18.07	-2.49
Forest to open grassland	5.49	1.16	7.75	7.50	0.56	3.26	0.86	-7.33	2.46	-0.36
Forest to sparse grassland	0.89	2.11	1.69	8.36	2.50	4.59	1.36	-7.46	2.38	-0.33
No Change	86.17	0.81	78.93	7.39	82.87	3.71	85.70	-7.40	77.08	-0.78

Table 6: Land cover and LST changes

In the afternoon built-up land cover had the lowest LST in 2005 and 2011, while in 2017 it was slightly higher than forest land cover (Figure 7c). During the day, built-up areas absorb incoming radiation, emitting it at night in long-wave radiation, hence having a higher night LST than open and sparse grassland.

High negative temperature changes were experienced between the years 2005 and 2011 while high positive temperature changes occurred between the years 1995 to 2000. 'No change' areas, where no change in land cover occurred had the largest percentage in areas. Land cover that showed significant changes in area and LST are those that changed from vegetated to built-up compared to 'forest to open grassland' and 'forest to sparse grassland'. This indicates that type of land cover change does have a corresponding effect on LST (Table 6). Negative values were obtained in 2005-2011 as LST in 2005 was higher than LST in 2011. The same trend occurred in 2011-2017. The change in the type of vegetation also has an effect on the LST. Forest to sparse grassland had lower percentage change in area between 1986 and 2005 than forest to open grassland. However the LST change was higher and this can be attributed to the physical characteristics of bare grounds with incoming radiation.

Changes in land cover had an effect on mean albedo in Upper Hill, where higher LST was associated with high albedo values and lower LST with low albedo values (Table 7).

	Built-up	Forest	Open grassland	Sparse grassland	Water
Albedo	0.16	0.15	0.18	0.18	0.09
LST (°C)	27.5	26.3	27.4	27.9	25.1

Table 7: Mean albedo and LST for each land cover

Water, having the lowest albedo, had the lowest mean LST in Upper Hill, whereas sparse and open grassland having high LST with corresponding high albedo mean values. This indicated that converting vegetated areas into impervious surfaces causes a shift in the local climate. Therefore, the local energy budget is controlled by the albedo, making it an important parameter in the urban heat island studies (Trlica *et al.*, 2017). The amount of solar insolation is reflected back into the atmosphere is determined by the albedo (Odunuga & Badru, 2015).

Figure 8 shows that forest land cover had the highest negative contribution index indicating that it does not contribute to the increased LST but instead reduces the surface temperature. However, its CI decreased from -0.40 in 1986 to -0.15 in 2017. This could be attributed to a reduction in percentage coverage in the area (Table 3).

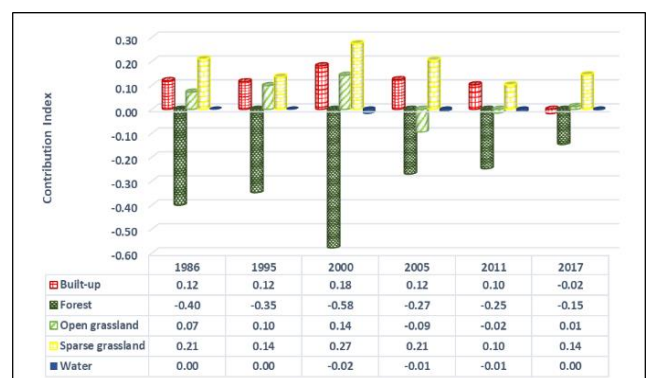


Figure 8: Contribution index of land cover

Sparse grassland had the highest positive contribution index indicating that it contributed to the increased surface temperature over Upper Hill (Figure 8). Water land cover did not show any significant contribution in 1986 and 1995. However, between the years 2000 and 2005 it had negative values of -0.02 and -0.01, indicating it had a cooling effect over the surface. Open grassland has a positive contribution index between 1986 and 2000 indicating that it had an overall warming effect over the land as it was higher than the mean LST over Upper Hill. In 2005 and 2011, it has a negative contribution index of -0.09 and -0.02 respectively, indicating that it had a lower surface temperature than the mean LST over Upper Hill. Built-up land cover has a positive contribution index from 1986 to 2011. However in 2017, it has a negative contribution index of -0.02 due to increased impervious surfaces which increases the thermal storage of the area (Yang *et al.*, 2017). Built-up land cover, during the day, absorbs and stores thermal energy resulting to negative contribution index.

4. CONCLUSION

This paper investigated the relationship between changes of land cover on land surface temperature and its effect on the contribution index. Multi-temporal satellite imagery are important in change detection and analyzing patterns of development, which enables planning decisions based on environmental conditions. The study was limited to analyzing imagery available during the warmer periods of the year but not the colder seasons due to cloud cover. The study determined that policy changes on built-up development have encouraged expansion of urban areas. This has mostly affected vegetated land cover with its reduction with increased urban development. Zoning policies in urban areas should consider performance zoning that would ensure that development does not occur at the detriment of vegetated land cover. There is need for a comprehensive environmental management plan in urban areas that would handle issues of greening in urban areas. Open spaces are important in urban areas and there is need of their protection and maintenance due to their importance in mitigating effects of heat islands. Forest land cover has experienced the greatest percentage decrease corresponding to increases in built-up density, resulting to a corresponding increase in LST. Increases in temperature occur where land cover changes from vegetated to impervious surfaces due to increases in mean albedo. Albedo influences the land surface temperature with vegetated areas having a lower albedo than built-up areas. Surface albedo is thus an important parameter in the studies of urban heat island as it affects the surface energy budget of a material. The interaction between land cover and incoming radiation is affected by the time of day due to the inherent characteristics of the land cover. It is therefore important to analyze both day and night surface temperatures to determine the relationship between material type and LST. This is comparable with Zhao *et al.*, (2015) where high albedo roofing materials in urban areas provide a cooling effect. Reducing the urban greenness of a city can have adverse effects and its potential effects can be determined on its residents from the contribution index. Increasing built-up densities increases the thermal storage within urban areas, resulting to warmer nights. Water bodies and tree cover are important as they reduce the surface and ambient temperature of an area. Analyzing the interaction of land cover and incoming radiation at different times of the day ensures a better understanding of the dynamics that changing landscapes can have

on the thermal comfort of urban residents, and impacts of climate change.

REFERENCES

- Bhargava, A., & Bhargava, S. (2018). Effects of Albedo in Urban Planning - Special Reference to Building Roofs. Examines Mar Biol Oceanogr., 1(2), 6–7. <https://doi.org/10.31031/EIMBO.2018.01.000506>
- Carmin, J., Nadkarni, N., & Rhie, C. (2012). Progress and Challenges in Urban Climate Adaptation Planning: Results of a Global Survey, 33. Retrieved from http://resilient-cities.iclei.org/fileadmin/sites/resilient-cities/files/Resilient_Cities_2012/Urban_Adaptation_Report_23_May2012.pdf
- Cristóbal, J., Jiménez-Muñoz, J. C., Prakash, A., Mattar, C., Skoković, D., & Sobrino, J. A. (2018). An Improved Single-Channel Method to Retrieve Land Surface Temperature from the Landsat-8 Thermal Band. Remote Sensing, 10(3). <https://doi.org/10.3390/rs10030431>
- Feizizadeh, B., & Blaschke, T. (2013). Examining Urban heat Island Relations to Land Use and Air Pollution: Multiple Endmember Spectral Mixture Analysis for Thermal Remote Sensing. IEEE Journal of Selected Topics in Applied Earth Observations and Remote Sensing, 6(3), 1749–1756. <https://doi.org/10.1109/JSTARS.2013.2263425>
- Firl, G. J., & Carter, L. (2011). Lesson 10 : Calculating Vegetation Indices from Landsat 5 TM and Landsat 7 ETM + Data. Natural Resources Ecology Laboratory, Colorado State University.
- Karanja, F. N., & Matara, S. (2013). The Transformation from Green to Concrete Cities; A Remote Sensing Perspective. International Archives of the Photogrammetry, Remote Sensing and Spatial Information Sciences - ISPRS Archives, 40(1W1), 163–166. Retrieved from <http://www.scopus.com/inward/record.url?eid=2-s2.0-84924739749&partnerID=tZOtx3y1>
- Koukoulas, S., Vafeidisa, A. T., Vafeidis, G., & Symeonakis, E. (2008). The Role of Spatial Metrics on the Performance of an Artificial Neural-Network Based Model for Land Use Change. The International Archives of the Photogrammetry, Remote Sensing and Spatial Information Sciences, 37(1), 1661–1666.
- Li, Y., Zhao, M., Motesharrei, S., Mu, Q., Kalnay, E., & Li, S. (2015). Local Cooling and Warming Effects of Forests Based on Satellite Observations. Nature Communications, 6, 1–8. <https://doi.org/10.1038/ncomms7603>
- Mbogo, E., Inganga, F., & Maina, J. (2015). Drought Conditions and Management Strategies in Kenya. Nairobi. Retrieved from http://www.ais.unwater.org/ais/pluginfile.php/629/mod_page/content/6/Senegal_EN.pdf
- Mwangi, P. W., Karanja, F. N., & Kamau, P. K. (2018). Analysis of the Relationship between Land Surface Temperature and Vegetation and Built-Up Indices in Upper-Hill, Nairobi. Journal of

- Geoscience and Environment Protection, 06(01), 1–16. <https://doi.org/10.4236/gep.2018.61001>
- Mwangi, P. W., Karanja, F. N., Kamau, P. K., & Letema, S. C. (2020). Impact of Urban Forms on 3D Built-up Intensity Expansion Rate from Aerial Stereo-Imagery. *ISPRS Annals of the Photogrammetry, Remote Sensing and Spatial Information Sciences*, V-4–2020, 6. <https://doi.org/10.5194/isprs-annals-V-4-2020-203-2020>
- Odunuga, S., & Badru, G. (2015). Landcover Change, Land Surface Temperature, Surface Albedo and Topography in the Plateau Region of North-Central Nigeria. *Land*, 4(2), 300–324. <https://doi.org/10.3390/land4020300>
- Schipper, L., Liu, W., Krawanchid, D., & Chanthay, S. (2010). Review of Climate Change Adaptation Methods and Tools. MRC Technical Paper No. 34, (34), 76. Retrieved from <http://www.mrcmekong.org/assets/Publications/technical/Tech-No34-Review-of-climate-change.pdf>
- Soudoudi, S., Wesonga, J. M., Matsaba, E. O., Njoroge, J. B., & Adimo, A. O. (2018). Attenuation Effect of Plant Canopy Sizes on Microclimate in Urban Greenspaces within Nairobi City, Kenya. *African Journal of Plant Science*, 12(7), 129–140. <https://doi.org/10.5897/ajps2018.1659>
- Tian, F., Qiu, G. Y., Yang, Y. H., Xiong, Y. J., & Wang, P. (2012). Studies on the Relationships between Land Surface Temperature and Environmental Factors in an Inland River Catchment based on Geographically Weighted Regression and MODIS Data. *IEEE Journal of Selected Topics in Applied Earth Observations and Remote Sensing*, 5(3), 687–698. <https://doi.org/10.1109/JSTARS.2012.2190978>
- Trlica, A., Hutyra, L. R., Schaaf, C. L., Erb, A., & Wang, J. A. (2017). Albedo, Land Cover, and Daytime Surface Temperature Variation Across an Urbanized Landscape. *Earth's Future*, 5(11), 1084–1101. <https://doi.org/10.1002/2017EF000569>
- U.S. Geological Survey (USGS), & National Aeronautics and Space Administration (NASA). (2016). *Landsat 8 (L8) Data Users Handbook*. America (2nd ed., Vol. 8). <https://doi.org/http://www.webcitation.org/6mu9r7riR>
- Vogelmann, J., Howard, S. . . , Yang, L., Larson, C. . . , Wylie, B. . . , & Driel, N. (2001). Completion of the 1990s National Land Cover Data Set for the Conterminous United States from LandSat Thematic Mapper Data and Ancillary Data Sources. *Photogrammetric Engineering & Remote Sensing*, 67(June), 13. <https://doi.org/10.1007/978-94-011-4976-1>
- Voogt, J. A. (2007). How Researchers Measure Urban Heat Islands. *Department of Geography*, 34. Retrieved from http://epa.gov/heatisland/resources/pdf/EPA_How_to_measure_a_UHI.pdf
- Wu, C.-D., & Lung, S.-C. C. (2016). Application of 3-D Urbanization Index to Assess Impact of Urbanization on Air Temperature. *Scientific Reports*, 6, 24351. <https://doi.org/10.1038/srep24351>
- Yang, X., Li, Y., Luo, Z., & Chan, P. W. (2017). The Urban Cool Island Phenomenon in a High-Rise High-Density City and its Mechanisms. *International Journal of Climatology*, 37(2), 890–904. <https://doi.org/10.1002/joc.4747>
- Zhao, Q., Myint, S. W., Wentz, E. A., & Fan, C. (2015). Rooftop surface temperature analysis in an Urban residential environment. *Remote Sensing*, 7(9), 12135–12159. <https://doi.org/10.3390/rs70912135>